Understanding synergetic effects of Zn and Rh-Cr promotion to wide-bandgap Ga, Ta and Ti oxides in photocatalytic water splitting

Antonio Bazzo[a] and Atsushi Urakawa*[a]

Promotion of semiconductor metal oxides by specific chemical elements is a widespread approach to enhance photocatalytic water splitting activity. Extraordinary boosting in the activity has been recently reported by Zn (dopant) and Rh-Cr (co-catalyst) promotion to Ga-oxide based photocatalysts. Herein, we report the general applicability of the effectiveness of the promotion strategy used for Ga oxides to Ta and Ti oxides in water splitting under UV irradiation using a slurry reactor. Photophysic characterization (photoluminescence and its decay) was used to clarify the specific roles of Zn and Rh-Cr and their synergetic catalytic action. Our experiments indicate that Zn acts as a booster of charge separation lifetime. Zn-promotion alone, however, does not trigger a great boost in catalytic activity in absence of Rh-Cr. Only when Rh-Cr is added the charge separation boost is fully exploited and driven within the catalyst towards overall water splitting. Effective wavelength ranges of excitation UV light source were also investigated in detail, leading to questioning the dominant semiconductor bandgap model for this class of catalysts.

Introduction

Photocatalytic water splitting is regarded as one of the best means to produce hydrogen using renewable energy sources. The use of semiconductor oxide powders as catalyst suspended in water is the most studied method for this aim.[1-3] By the end of the 20th century, the efficiency of artificial photosynthesis had improved relatively slowly and most reports focused on Ti-based materials.[2, 4] Recently, new classes of materials have been reported, showing outstanding activity towards overall water splitting. $NaTaO_3$ and GaN:ZnO are among the most prominent examples with drastic activity improvements.[5, 6] Notably, unprecedented high activity in a slurry reactor under batch operation was reported by Sakata and co-workers using gallium oxide based materials as wide bandgap semiconductor photocatalysts.[7-9] Doping with zinc (2<x<6 mol% w.r.t. gallium oxide) was shown highly beneficial, resulting in up to one order of magnitude increase in water splitting activity from a few hundreds $\mu mol \cdot g_{cat}^{-1} \cdot h^{-1}$ of hydrogen evolution of the undoped gallium oxides. The water splitting activity was further enhanced by modifying the zinc-doped material with the previously reported nickel oxide or rhodium-chromium based co-catalysts.[10] To our knowledge Ga_2O_3 doped with Zn and promoted with Rh-Cr promotors (i.e. Rh-Cr/Zn-Ga_2O_3) exhibits one of the highest overall water splitting activity, reaching the production rate of 21 $mmol \cdot g_{cat}^{-1} \cdot h^{-1}$ for H_2 and 10.5 $mmol \cdot g_{cat}^{-1} \cdot h^{-1}$ for O_2 without sacrificial agents.[7]

In this work, we aim to (i) investigate the general validity of the promotional strategy using Zn and Rh-Cr for water splitting, (ii) examine the activity of Zn- and Rh-Cr- promoted materials in CO_2 reduction, and importantly (iii) elucidate the role of Zn and Rh-Cr promotors. Ga_2O_3, Ta_2O_5, $NaTaO_3$ and TiO_2 were used as starting materials. A slurry reactor was used and H_2 and O_2 concentrations were quantified by mass spectrometry (MS) which was calibrated by gas chromatography (GC). The use of MS allows detecting product concentrations at high time resolution (order of seconds) and identifying activity features varying within a short time-frame.[11] In order to test the possibility to drive CO_2 reduction to gaseous products alongside water splitting, CO_2 was used as carrier gas throughout this work. Insights into the promotional effects were studied by photophysic techniques such as diffuse reflectance UV-Vis spectroscopy, photoluminescence (PL) spectroscopy and PL decay. The last technique was used to uncover the influences of the promotors on the lifetime of electrons and holes generated by photo-excitation in the bulk and at the surface of catalyst materials. The combination of these characterization techniques together with the activity tests allowed identifying the key roles of Zn and Rh-Cr promotors and inferring a general mechanism of synergetic positive effects for photocatalytic water splitting.

Experimental Section

Catalyst preparation

β-Ga_2O_3 (Sigma-Aldrich), β-Ta_2O_5 (Alfa-Aesar), and P25 titania (Degussa) were used as raw materials. The starting white powders were calcined at 773 K in air for 3 h prior to use. 2 wt% Zn (5.7 mol% w.r.t. Ga_2O_3) doping and Rh-Cr (0.5 and 0.75 wt% respectively) co-deposition on solid powders were performed by the wet impregnation procedure. An aqueous precursor solution ($Zn(NO_3)_2 \cdot 6H_2O$ or $RhCl_3$ + $Cr(NO_3)_3 \cdot 9H_2O$; each 500 $\mu L \cdot g_{cat}^{-1}$) was added to the material and mixed in a glass container until a homogeneous slurry was obtained. The slurry was then homogenised by means of water bath ultrasonication cycles (3 min each), alternating with further mixing to improve the homogeneity. The slurry was then dried at 363 K, crushed, and finally calcined at 1123 K for 6 h (Zn-doping), and/or at 623 K for 1 h (Rh-Cr promotion) under the flow of synthetic air (10 $mL \cdot min^{-1}$).

Continuous flow photocatalytic reaction setup

The reaction setup (Fig. 1) is an upgrade of a previously reported in-house developed system.[11] In the order of the path along the gas flow, the system is equipped with (1) gas supply system controlled by mass flow controllers (MFCs, Bronkhorst) to feed gaseous CO_2 or a calibration gas mixture, (2) slurry photocatalytic reactor, (3) high pressure mercury UV light source equipped with programmable on/off switch, (4) water-cooled trap to condense liquids from the gas stream and avoid their sampling by GC and MS, (5) MS (Pfeiffer Vacuum, Omnistar GSD 320), and (6) GC (Agilent Technologies, micro GC 490). The slurry reactor was a vessel consisting of two pieces. The bottom part was a round bottom tubular piece made of UV transparent quartz with the volume of 35 mL, which was joined by means of ground glass cones to a glass head (providing 36.5 mL headspace) equipped with GL13 screw inlet and outlet. The carrier gas (CO_2) at 4.5 $mL \cdot min^{-1}$ was bubbled through the liquid slurry containing water and catalyst powder at the bottom of the reactor through a glass capillary (ID: 2 mm). A powder catalyst (20 mg, 0.57 $g \cdot L^{-1}$) was suspended in

Type-I ultrapure water (35 mL, Milli-Q) and kept under agitation by means of a magnetic stirrer. In order to facilitate homogeneity of the suspension and dissolution of agglomerates, the reactor was briefly dipped in an ultrasound bath prior to catalytic tests. The gaseous products were analysed by the MS. Calibration of product concentrations obtained by MS values was performed by the on-line micro GC, injecting few samples at different times during the catalytic run. The light source was a 400 W high-pressure Hg lamp (UV-technik), regulated to a source power of 200 W by means of a dimmable electronic ballast (Solux).

Reaction procedure

At MS signal stabilisation, the lamp was switched on and the evolution of reaction products was followed by MS. Monitored mass-to-charge ratios (m/z) were chosen to avoid overlaps as much as possible, and they are as follows: hydrogen (H_2 : m/z = 2), methane (CH_4 : m/z = 15), oxygen (O_2 : m/z = 32). The reaction was terminated by switching off the lamp. The reaction temperature was approximately 338 K, which was the equilibrium temperature upon irradiation. A FS window (6 mm thickness) was used as a filter, buffering the high heat delivered by the lamp which would, otherwise, cause excessive water evaporation from the slurry. Alternatively, BK7 (Eksma optics) and FGUVS11 (Thorlabs) optical filters were used to study the effect of excitation wavelength on the catalytic activity.

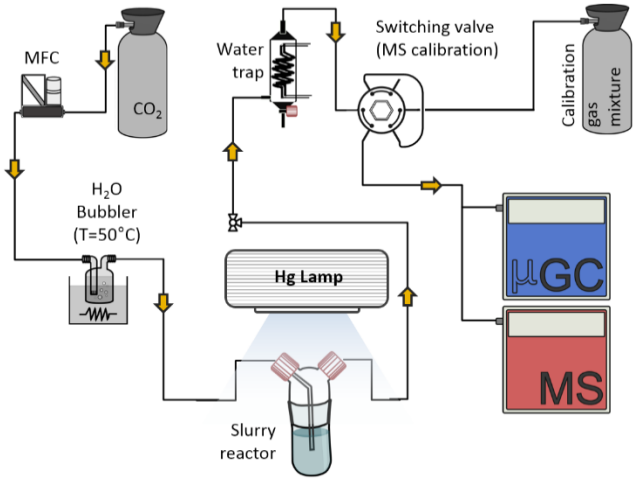

Fig. 1 Continuous photocatalytic reaction system.

UV-Vis diffuse reflectance measurements

UV-Vis diffuse reflectance measurements were performed on a Shimadzu UV-2401PC spectrophotometer equipped with a PMT detector, double beam optics, D_2 and W light sources, and an ISR 240 A 60 mm integrating sphere. Powder samples were loaded on a round window (fused silica) holder with ca. 1 mm material thickness. Spectra were collected in 200-800 nm range using $BaSO_4$ as reflectance standard. E_g values were estimated by fitting the linear range of the slope change in Kubelka-Munk unit (KM(λ), arbitrarily normalized) and intersecting it at KM(λ) = 0.

Photoluminescence measurements

Fluorescence measurements were performed on a Aminco-Bowman Series 2 Luminescence spectrofluorimeter equipped with a high voltage PMT detector and a continuum 150 W Xe light source as well as a pulsed 7 W Xe lamp allowing PL decay lifetime measurements in the t >90 μs range. Solid powder samples were loaded in a fused silica cuvette bearing a sample pocket (100 μm deep). The cuvette was mounted on a variable angle solid support accessory allowing light sampling at the incident angle of 68°. Emitted light was filtered with a BK7 borosilicate window to avoid the intense visible range harmonics, originating from the UV excitation reflection. All the measurements were performed at room temperature in air. PL decay traces vs. time were fitted with an exponential equation in the form $y(t) = y_0 + A_1 e^{-t/\tau 1} + A_2 e^{-t/\tau 2}$.

Results and Discussion

Zn and Rh-Cr promotion and structural change

Promotional effects were studied using a modular approach to unravel how the single promoter (Zn or Rh-Cr) affects the photocatalytic activity. More precisely three different materials were prepared by modifying commercial metal oxides (M_xO_y) as follows.

0 Bare M_xO_y, calcined at 773 K
1 Zn (2 wt%) impregnation to **0**, calcination at 1123 K for 6 h (*doping*)
2 Rh (0.5 wt%) - Cr (0.75 wt%) co-impregnation to **0**, calcination at 623 K for 1 h (*co-catalyst deposition*)
1+2 Zn (2 wt%) and Rh (0.5 wt%) - Cr (0.75 wt%) promotion following steps **1** and **2** consecutively (*doping and co-catalyst deposition*)

Fig. 2 shows the effects of Zn doping and Rh-Cr deposition on the Ga_2O_3, Ta_2O_5 and TiO_2 crystal structures. The pristine Ga_2O_3 material was identified as monoclinic β-Ga_2O_3 (Fig. 2, top section).[12] Upon Zn doping the main characteristics of crystal structure remain unchanged except for three reflections at 29.0, 35.7, and 63.2° (Fig. 2, * symbol). The reflection at 35.7° was previously assigned by Sakata[8] as due to the formation of ZnO/Ga_2O_3 mixed oxide, i.e. $ZnGa_2O_4$. Hence this is the key signature of the incorporation of zinc into the structure of gallium oxide. Another expected signature, according to the same reference, is the reflection peak shift of (202) plane ($2\theta = 31.7°$) to lower angles by the substitution of some Ga^{3+} ions (0.060 nm) with larger Zn^{2+} ions (0.069 nm). However, this shift was not observed for our samples. Similarly, the main structural features of β-Ta_2O_5 does not change upon Zn doping (Fig. 2, middle section). Nevertheless a number of new reflections are visible in the $16 < 2\theta° < 36$ range after step 1 (e.g. Fig. 2, ◊ symbol). They are attributed to $ZnTa_2O_5$ (zinc metatantalate) polymorphic structure[13], thus confirming Zn incorporation into the structure of tantalum oxide.[14, 15] In contrast, high temperature treatment on TiO_2 yields a different outcome. No signature of Zn incorporation can be identified, but the starting material (P25, anatase/rutile ≈ 3/1 mixture)[16, 17] undergoes a complete structural change to rutile after step 1. This change is in agreement with the well-known anatase-rutile phase transformation[14, 15] even in presence of Zn. [14, 15 14, 15 14, 15 14, 15 14, 15 14, 15 14, 15 14, 15]
No effect of Rh-Cr impregnation is visible in the XRD patterns (therefore, those of the samples after step 2 is not shown in Fig. 2) and the same structural characteristics of parent non-Rh-Cr-doped materials are retained. This is explained by low metal loading and low temperature treatment which are likely insufficient to drive any detectable phase transformation and formation of new crystalline phases.

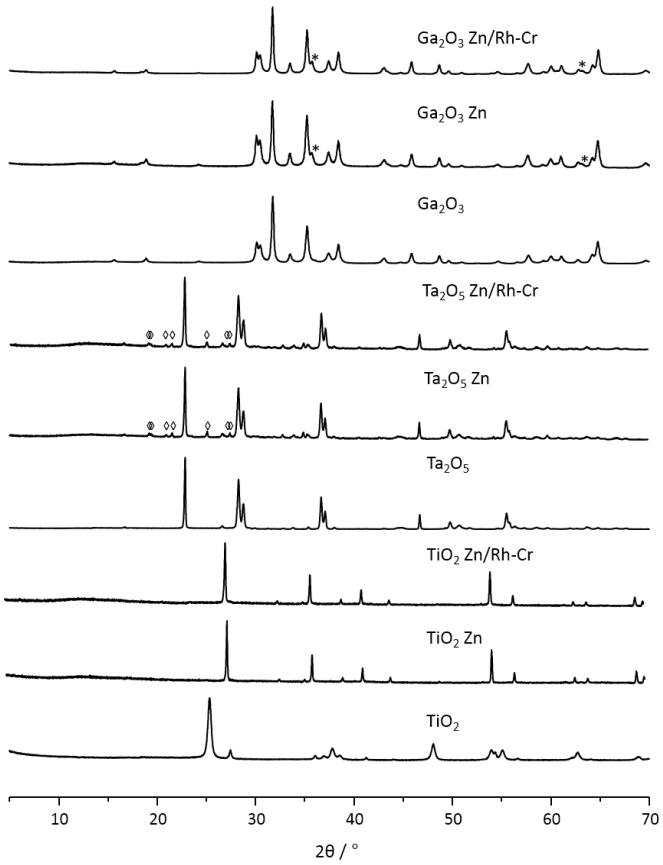

Fig. 2 XRD patterns of Ga_2O_3, Ta_2O_5 and TiO_2 and after Zn and Zn/Rh-Cr promotion. The symbols * (Ga_2O_3) and ◊ (Ta_2O_5) highlight the key signatures due to Zn doping.

Slurry reactor testing of Ga, Ta and Ti based photocatalysts

The prepared materials at the four different promotion levels (**0**, **1**, **2**, **1+2**) were tested in a continuous flow slurry reactor. CO_2 was used as the carrier gas to probe the possibility of parallel photocatalytic CO_2 reduction besides water splitting. No particular influence of CO_2 on water splitting activity was ensured by comparing the activity with that obtained using N_2/Ar as the carrier gas.

Figs. 3 and 4 show H_2 and O_2 concentration profiles obtained during the photocatalytic tests of Ga_2O_3-based materials. Clearly, the Zn doping and Rh-Cr co-catalyst deposition drastically improved the photocatalytic activity. The base activity of Ga_2O_3 for H_2 production was enhanced by 6 times by Zn doping and by 9 times with Rh-Cr co-catalyst deposition. H_2 productivity was increased roughly 50 times by Zn/Rh-Cr promotion. The results suggest a strong synergetic promoting effect between the doping and the co-catalytic components, which cannot be explained by simple additive combination of the two contributions. The catalytic activities reported here are in good agreement with those reported for Sakata's commercial Ga_2O_3 modification series[7] (ca. 50% of the reported batch reactor activity for Zn/Rh-Cr modified sample) with the exception of a lower oxygen evolution for bare Ga_2O_3 and Ga_2O_3 Zn samples in our study (very close to the detection limit as shown in Table 1), although differences in reactor design, catalyst amount and lamp power do not allow a strict comparison. Contrary to findings disclosed in literature, our data suggest that only the Rh-Cr loaded catalysts are capable of continuous stoichiometric oxygen evolution, i.e. resulting in sustained overall water splitting.

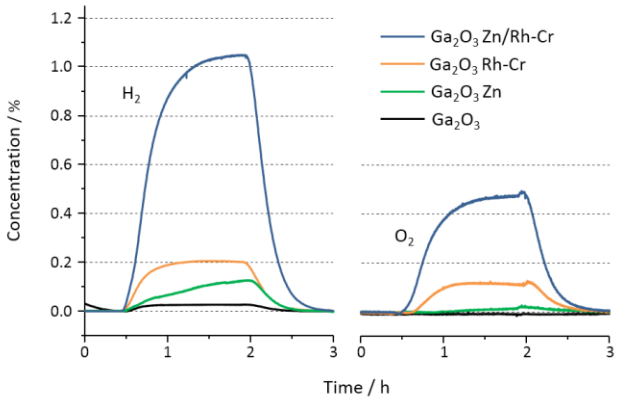

Fig. 3 H_2 and O_2 concentration profiles with the unpromoted and promoted Ga_2O_3 catalysts in the continuous flow slurry reactor under 1.5 h UV (high pressure Hg lamp) irradiation (ON at 0.5 h, OFF at 2 h).

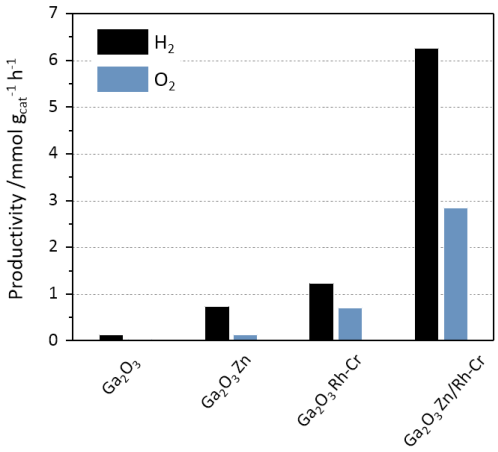

Fig. 4 Comparison of H_2 and O_2 steady state productivity of the Ga_2O_3 based catalysts.

The modular approach of the Zn doping and Rh-Cr co-catalyst modification was evaluated for other classes of promising metal oxide photocatalysts in order to investigate its general efficacy. Titanium oxide (TiO_2, P25) was chosen as a second reference material because of the widely reported activity and our previous experience.[11] As a third subject of comparison, tantalum oxide (Ta_2O_5) was selected because high photocatalytic water splitting activity was reported in presence of a suitable co-catalyst (e.g. NiO, Ru_2O, Rh/Cr).[18-21]

Both bare titanium and tantalum oxides could produce hydrogen upon UV irradiation in presence of water. On the contrary, oxygen evolution was not observed under the reaction conditions of our study. Strikingly, residual oxygen concentration was observed to drop from the base O_2 concentration level (an example with Ta_2O_5 is shown in Fig. 5) in the gaseous effluent stream after the photocatalytic reactor. The tightness of the system was ensured to the best extent (no detectable leakage), but a very small amount of oxygen seems to be present. This is common for continuous flow systems especially when low flow rate is used with negligible inner over pressure. Oxygen should not be considered a flow component, rather a small diffusion contamination resulting from imperfect sealing of the flow system. Nevertheless, this imperfection allows us to clearly show that: i) when the catalyst is capable of evolving oxygen, an oxygen contamination does not quench the reaction, ii) when the catalyst is not capable of evolving oxygen, consumption can be detected instead, iii) oxygen evolution and consumption probably occur independently on different surface reaction sites. The drop in O_2 concentration was transient; the oxygen level was restored to the base level before irradiation. It is possible that, instead of molecular oxygen, a variety of oxygen species (radical or with intermediate oxidation state) might be formed from O^{2-} ions as alternative oxidation reaction product.

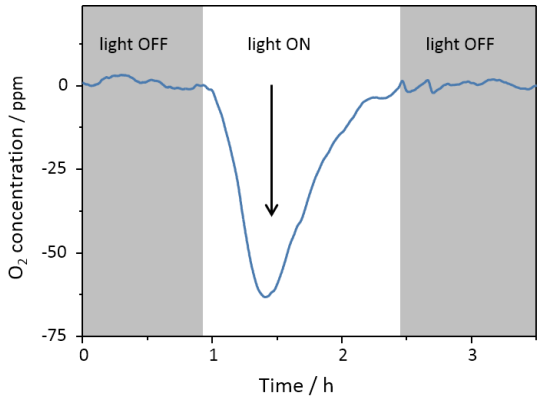

Fig. 5 Residual oxygen consumption using Ta_2O_5 catalyst and upon irradiation. Baseline oxygen concentration has been subtracted to show only the reaction contribution.

Furthermore bare (**0**), Zn doped (**1**), Rh-Cr deposited (**2**), and Zn/Rh-Cr doped/deposited (**1+2**) Ta_2O_5 and TiO_2 materials were prepared and tested under the same condition as described for the Ga_2O_3 based materials. The steady state productivity are displayed in Fig. 6 and listed in Table 1.

Cleary, the promotion effects provided by Zn and Rh-Cr on hydrogen productivity were consistently observed in a very similar fashion as observed for the Ga_2O_3 series. Moreover, upon Rh-Cr modification the sign of the mentioned negative oxygen productivity is reversed for the Ta_2O_5-based materials confirming even more strongly the boosting of oxygen evolution observed previously for gallium oxide series. The addition of Rh-Cr effectively blocks the oxygen consumption and triggers its production.

The synergetic activity boosting provided by Zn and Rh-Cr combination is again observed for Ta_2O_5 series, whereas in case of TiO_2 series the boosting level appears to be more close to a simple addition of Zn and Rh-Cr promotion effects. This may be partially caused by the phase transition of the base titania upon Zn-doping to the less active rutile phase (Fig. 2). Nevertheless, the Zn and Rh-Cr promotion effects overcome the negative effect of the phase transformation, improving the net activity. Among the Ta_2O_5 series tested, the best catalyst yields approximately 10% of the activity observed for Ga_2O_3 Zn/Rh-Cr catalyst, whereas the best catalyst of the TiO_2 series shows a significantly lower activity, about 250 times less than Ga_2O_3 Zn/Rh-Cr (Table 1).

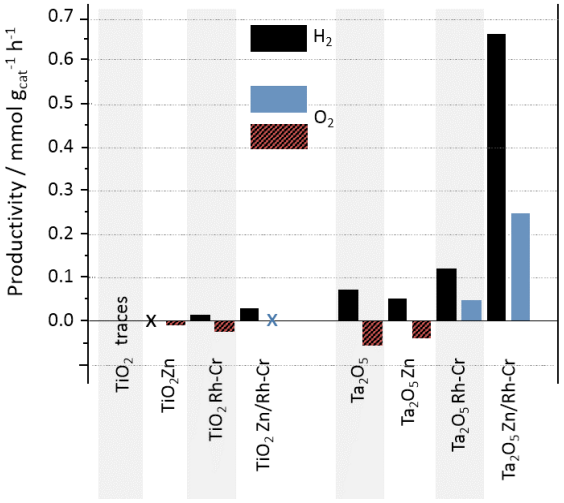

Fig. 6. Comparison of H_2 and O_2 steady state productivity measured for TiO_2 and Ta_2O_5 based catalysts. Dashed red bars represent negative productivity for oxygen: these values were calculated from the value of maximum negatively dip of oxygen concentration upon irradiation. These values should be taken as a semi-quantitative indication of the oxygen consumption, which appears to be a transient phenomenon and not a steady one.

Table 1 H_2 and O_2 productivity for the Zn and Rh-Cr promoted Ga, Ta, Ti oxides. The important data are displayed graphically in Figs. 4 and 6.

Catalyst	Productivity ($mmol \cdot g^{-1} \cdot h^{-1}$)	
	H_2	O_2
Ga_2O_3	0.13	0.04
Ga_2O_3 Zn	0.75	0.13
Ga_2O_3 Rh-Cr	1.23	0.70
Ga_2O_3 Zn/Rh-Cr	6.27	2.84
Ta_2O_5	0.07	-0.06
Ta_2O_5 Zn	0.05	-0.04
Ta_2O_5 Rh-Cr	0.12	0.05
Ta_2O_5 Zn/RhCr	0.66	0.25
TiO_2	*traces*	0.00
TiO_2 Zn	0.01	-0.01
TiO_2 Rh-Cr	0.01	-0.02
TiO_2 Zn/Rh-Cr	0.03	0.00

In all cases, products by CO_2 reduction (e.g. CO, CH_4) was never observed in the gas phase.

Bandgap measurements and excitation wavelength dependence on photocatalytic activity

Table 2 summarizes the bandgap analysis on the Ga, Ta, and Ti oxide-based materials calculated by the Tauc method (Fig. S1, Table S1 in Supporting Information). Bandgap comparison among the three material families allows us to first order the bandgap values in ascending scale as follows: titanium oxide (2.87 - 3.25 eV), tantalum oxide (3.71 - 3.86 eV), and gallium oxide (4.28 - 4.59 eV). These values are in good agreement with literature data.[21-25] Within the same family, the pure oxides of Ti, Ta, and Ga display the widest bandgap. Interestingly, the modification with Rh-Cr always resulted in slight red-shift of the λ_{onset} value. This is the most evident for titania, resulting in +27 nm shift of the onset energy (-0.22 eV). The same material is even more affected by combined Zn doping, resulting in +50 nm shift (-0.38 eV). The phase transformation from anatase to rutile, upon Zn doping, is also an important contribution to this shift (typically 25 nm shift).[26] On the contrary, the bandgap of Ga and Ta oxides does not appear to change upon zinc doping. Only noticeable differences arise after Rh-Cr deposition (+13 and +20 nm for Ta and Ga oxides, respectively). This shift though can not be confidently interpreted as a change in bandgap of the material, as the low calcination temperature upon Rh-Cr deposition would not justify a structural change of the bulk of the material.

Table 2. Tauc plot derived λ_{onset} and corresponding E_g values (by the formula $E_g = 1240/\lambda_{onset}$).

Material	λ_{onset} /nm	E_g / eV
Ga_2O_3	270	4.59
Ga_2O_3 Zn	270	4.59
Ga_2O_3 Rh-Cr	290	4.28
Ga_2O_3 Zn/Rh-Cr	290	4.28
Ta_2O_5	321	3.86
Ta_2O_5 Zn	321	3.86
Ta_2O_5 Rh-Cr	334	3.71
Ta_2O_5 Zn/Rh-Cr	334	3.71
TiO_2	382	3.25
TiO_2 Zn	416	2.98
TiO_2 Rh-Cr	409	3.03
TiO_2 Zn/Rh-Cr	432	2.87

Indeed, the onset change likely derives from an extra, wide absorption feature to the spectra (Fig. S1), overlapping to the semiconductor band-to-band transition in the UV range but slowly diminishing its intensity towards the visible range and reaching up to the NIR region. It is this absorption feature responsible for the brownish colour of the material after Rh-Cr addition. Although some changes in the bandgap are recognized by modifying the material with Zn and Rh-Cr, the absolute shift in the bandgap values does not appear to be sufficiently relevant to justify the drastic changes in catalytic activity shown in the previous sections.

In order to further evaluate the dependence of photocatalytic activity on excitation wavelength, we performed catalytic tests with two different optical filters besides FS which is practically transparent to the spectrum of the UV lamp. We first used a borosilicate window (BK7), cutting off completely the spectrum below 300 nm, and then a black filter (BF; bandpass $275 < \lambda < 375$ nm), as a substitute to the secondary FS window placed between the UV lamp and reactor. The window change was performed without interrupting the irradiation. The filter effects on the activity of Ga_2O_3 Zn/Rh-Cr catalyst are shown in Fig. 7 (traces a). Upon changing to the BK7 filter the activity was fully suppressed. The negligible activity was sustained by subsequent switch to the BF. The high level of activity was restored reverting to the starting configuration with the FS filter ($t > 3.7$ h). These observations are in agreement with the semiconductor photocatalyst model because FS is the only material allowing irradiation at a wavelength of approximately 250 nm. The irradiation above 275 nm transmitted by BF or above 300 nm transmitted by BK7 was not sufficiently energetic to drive the water splitting reaction.

Ta_2O_5 has a smaller bandgap than Ga_2O_3. Water splitting activity using the BF is expected since the energy of UV light passing through this filter is higher than the bandgap of tantalum oxide. Against our expectations, both BK7 and BF filters acted similarly, fully suppressing the catalytic activity of the promoted Ta_2O_5 (Fig. 7 bottom, traces b), in a very similar fashion as observed for the gallium oxide based catalyst (Fig. 7, bottom, traces a). This implies that the semiconductor model might not be correctly describing the activity observed for tantalum oxide based materials. Rather, TaO_x^{n-} surface units could be responsible for the actual photocatalytic process, similar to the model described by Anpo and co-workers for TiO_4^{n-} units on titania.[27] The band structure, usually considered as the basis of the photocatalytic mechanism, might play a marginal role. This statement is also in agreement with the strikingly similar activity we observed for tantalum materials with different composition and structure (i.e. tantalum oxides and sodium tantalite, Fig. S2). Furthermore, it is not possible to exclude that the gallium oxide based materials also function in the same photocatalytic mechanism. The catalytic process, triggered by highly energetic UV light, might similarly depend on GaO_x^{n-} surface species rather than band transitions. The high E_g of gallium oxide does not allow to distinguish which pathway is active by the simple light filtering experiment performed here.

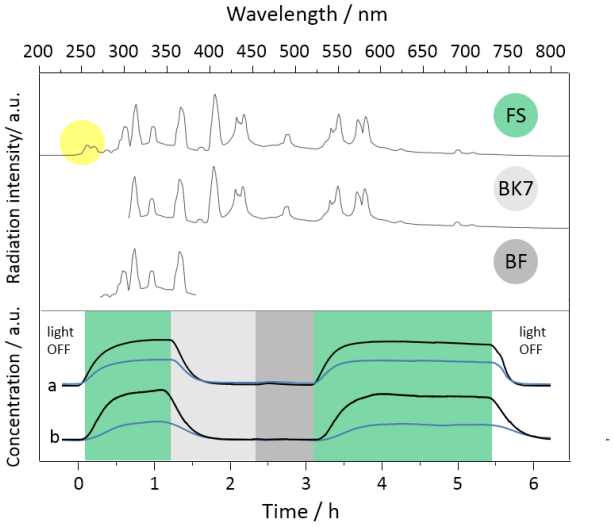

Fig. 7 [Upper section] Spectral component passing to reach photocatalyst using three types of optical filters: UV grade fused silica (FS, green), optical borosilicate (BK7, light grey), and a FGUV11S black filter (BF, deep grey). [Bottom section] H_2 (black) and O_2 (blue) concentration profiles (normalized to arbitrary values) under UV irradiation in the continuous flow slurry reactor under different optical-filtering conditions. Catalysts: a) Ga_2O_3 Zn/Rh-Cr and b) Ta_2O_5 Zn/Rh-Cr. The yellow circle highlights the apparent wavelength range activating both materials in water splitting.

Photoluminescence spectroscopy

Photoluminescence (PL) spectra (λ_{exc}= 265 nm) collected for the Ti, Ta, and Ga oxide based materials are shown in Fig. 8. For each family of the oxide materials, optical parameters of the measurements (e.g. bandpass slit opening and detector gain voltage values) were fixed, allowing comparison and semi-quantitative analysis. All materials were photoluminescent at RT in air. Their average absolute photoluminescence intensity followed the trend of Ga- > Ta- > Ti-oxides. We mostly focus on relatively high stoke-shift long-wavelength emissions, as they are most commonly related to the surface states responsible for radiative recombination pathways which are often linked to photocatalytic activity and mechanisms.[28, 29]

The emission observed from the titania-based samples (Fig. 8, top) can be ascribed to the overlap of band-to-band and exciton emissions; one centred at 410 nm, the other appearing as the multiple bands at >445 nm.[30] Also, it can be noticed that upon zinc doping, the short wavelength tail below 410 nm is substantially diminished.

This implies that Zn considerably suppresses the most energetic band-to-band recombination, consequently boosting the exciton emission component. Therefore we assigned the emission below 410 nm to the former origin. The latter can then be assigned, according to Liu et al.[28] to surface defects recombination and to bulk phonon coupled recombination in correspondence of the sharp peaks at 450-500 nm. For tantalum oxide-based samples (Fig. 8 middle), features very similar to the titania-based materials are present, but detailed interpretation seems too speculative due to very limited literature data available. Gallium oxide-based samples (Fig. 8 bottom) display a single emission feature centred at λ = 455 nm, with weak phonon coupling. Stoke shift is large (ca. 180 nm) and we can exclude the band-to-band nature of this emission. Similar simple emission features were reported in literature and assigned to electron hole recombination mediated by gallium or oxygen defects or vacancies.[31, 32]

When the relative intensity of the emission spectra for each family of catalyst is compared, clear trends can be recognized. A clear decrease in PL intensity is consistently observed upon addition of Rh-Cr co-catalyst. It should be noted that this effect might not be only due to modified PL features of the supporting semiconductors. Possibly, self-absorption phenomena might be also involved, since Rh-Cr absorption features overlap with the emission features of the supporting metal oxides (Fig. S1, Supporting Information). The most important trend emerging from this analysis is the clear boosting of PL intensity by Zn doping. The enhanced PL emission cannot be correlated with modification of absorption features for Ga and Ta oxides because the absorption characteristics do not sensibly change upon doping (*vide supra* and Fig. S1). This is an important indication of improved stability of charge separation states. From another point of view, Zn doping could be preventing electron-hole recombination pathways, which is certainly a desirable property as photocatalysts. The combined effects of Zn and Rh-Cr for the PL intensity are consistent for the Ga and Ta

oxides samples, in the following order: Zn > bare > Zn/Rh-Cr > Rh-Cr. The PL results appear to be more complex to be rationalized for TiO_2 materials, possibly due to the phase transformation of TiO_2.

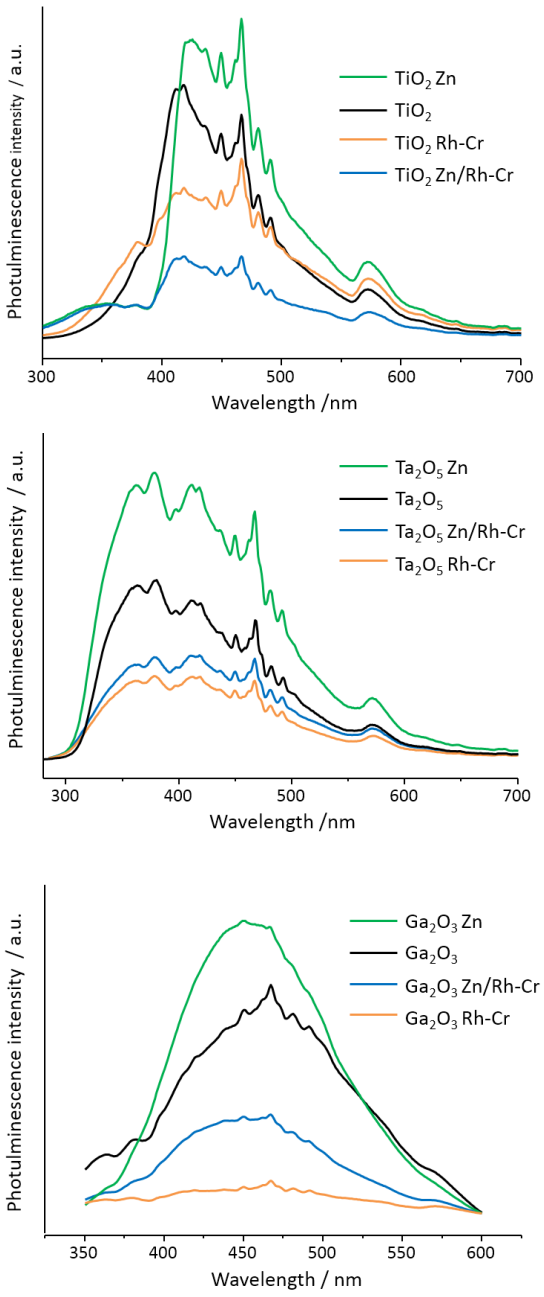

Fig. 8 Photoluminescence spectrum of TiO_2- Ta_2O_5- and Ga_2O_3-based materials. λ_{exc}= 265 nm.

PL decay

Furthermore, time-dependent PL spectroscopy was employed to shed light on the impacts of the promotors on the lifetime of generated electrons and holes upon photo-activation using Ga_2O_3-based materials. Fig. 9 shows PL decay curves for unpromoted gallium oxide and after promotion with Zn and/or Rh-Cr (λ_{exc} = 265 nm; λ_{emi} = 440 nm). The best fit to the PL decay curves was found using double exponential decay functions with millisecond scale decay τ

constants. Other Ta and Ti oxides materials were tested in the analogous way, but no decaying signal was detected, most likely due to faster decay in the microsecond range (the equipment only allowed sampling at t > 90 μs). Once again, zinc clearly makes a prominent difference in terms of emission decay properties. An order of magnitude increase in the lifetime (both τ_1 and τ_2) is observed upon zinc doping with an impressively long τ_2 = 21.7 ms for Ga_2O_3 Zn material as compared to τ_2 = 1.78 ms observed for bare Ga_2O_3. The similar time scale (1.2-2.0 ms) of τ_2 for the Ga_2O_3 materials and of τ_1 for the Ga_2O_3 Zn materials suggest that they may have the same physical origin and there was a creation of additional sites or mechanism retarding the PL decay upon Zn-doping.

According to the findings described in the previous section, zinc doping is highly beneficial to the emission properties of gallium oxide material, actively boosting radiative recombination and avoiding faster non-radiative recombination pathways. On the contrary, Rh-Cr addition appears to have a negative effect on lifetime (τ_2 = 1.36 ms on Ga_2O_3 Rh-Cr) as well as in terms of PL intensity as previously shown. This effect is highly noticeable for Ga_2O_3 Zn/Rh-Cr material (τ_2 = 12.4 ms), showing a 40% luminescence lifetime shortening as compared to the Zn-doped, Rh-Cr free material.

It is also worth mentioning that the overall decay times were surprisingly long. Analogous materials were reported in literature to display longest decay constants in the order of a hundred μs at 77 K.[31]

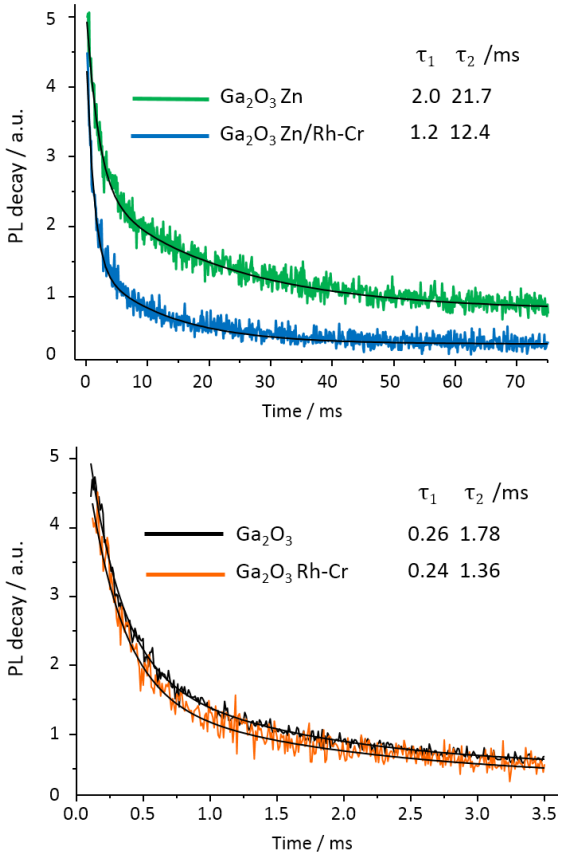

Fig. 9 Photoluminescence decay of zinc-doped (top) and non-zinc-doped (bottom) Ga_2O_3-based photocatalysts (λ_{exc} = 265 nm and λ_{emi} = 440 nm).

Understanding the effects of Zn doping and Rh/Cr deposition

Water oxidation to O_2 is generally perceived as a more difficult reaction than the reductive half-reaction to produce H_2. For this reason, water splitting reactions are often unbalanced in stoichiometry and often promoted by extensive use of sacrificial hole scavengers[1]. Particularly in the case of Ta_2O_5 poor stoichiometry was also reported by Takahara and co-workers[20].

Within the scope of this work, oxygen productivity is greatly affected by Zn and Rh-Cr promotion. Focusing on the Ta_2O_5-based catalysts, oxygen is consumed during the irradiation in the absence of Rh-Cr co-catalyst and it is conversely produced in its presence. In other words, the Rh-Cr co-catalyst plays a key role to complete overall water

splitting, promoting stoichiometric oxygen evolution. Bare and Zn-doped Ta_2O_5 materials are capable of H_2 evolution but do not appear to bear efficient catalytic sites for O^{2-} oxidation. Rather, the reaction appears to be suppressed by competing O_2 reduction. Oxygen is then possibly converted to (i) hydroxyl surface species or to (ii) peroxo or radical oxygen species (for example $O_2^{\bullet-}$, $HO^{\bullet}$, $HOO^{\bullet}$) released in the slurry, or simply (iii) back to water, reversing the water splitting activity. Many of these species are often reported in literature and considered active reactants in photocatalytic decomposition of organic compounds, when these catalysts are used for water purification or biomass transformation.[33-36] The capture or consumption of oxygen and the oxygen evolution reaction appear to be competitive phenomena occurring at different surface sites. Upon Zn doping to Ga_2O_3, the fivefold rise in hydrogen evolution is not accompanied by stoichiometric oxygen production (Fig. 4 and Table 1). However, as soon as the material is promoted with Rh-Cr, oxygen evolution is efficiently triggered. When Ga_2O_3 Rh-Cr and Ga_2O_3 are compared, O_2 production was enhanced up to the over-stoichiometric ratio (Fig. 4 and Table 1).

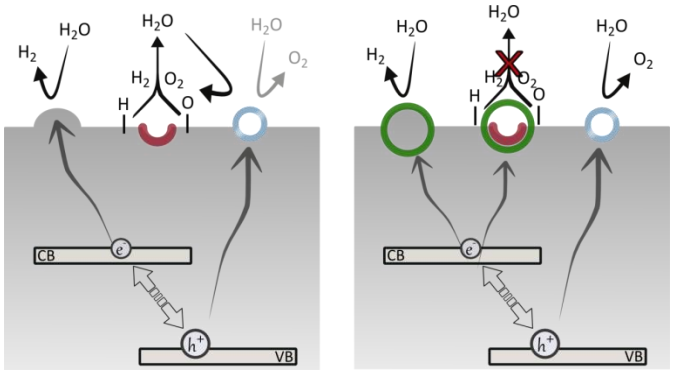

Fig. 10 Possible mechanistic scheme of Rh-Cr boosting effect. On the left, in absence of Rh-Cr, recombination sites are active (red); oxygen evolution sites (blue) are short circuited. On the right, Rh-Cr co-catalyst (green) inhibits the recombination sites and boosts H_2 and O_2 production at the same time.

Rh-Cr has been reported in literature to act as hydrogen evolution site, rather than oxygen one.[10, 37] Assuming this is valid, the oxygen evolution boosting effect of this co-catalyst may rely on a dual action. It might be working first as a very efficient electron trap and hydrogen evolution site and, at the same time, it might be blocking the surface oxygen recombination sites. The suppression of the recombination activity can lead to effective promotion of overall water splitting process (Fig. 10). TiO_2-based catalysts display very low activity for H_2 evolution as compared to Ta_2O_5 and Ga_2O_3-based catalysts. Apart from the absence of Zn/Rh-Cr synergetic effects, oxygen evolution is never detected in TiO_2-based materials, although the level of negative oxygen concentration becomes less with Zn and Rh-Cr promotion (Fig. 6).

According to the photophysic properties of the studied materials upon Zn and/or Rh-Cr modification, mechanistic models for the origin of PL and their mechanistic implications in photocatalytic water splitting can be outlined. Clearly, Zn doping accounts for both enhancement of PL intensity and decay time. On the contrary, Rh-Cr modification seems working in the opposite direction; lowering the PL emission as well as the PL decay time.

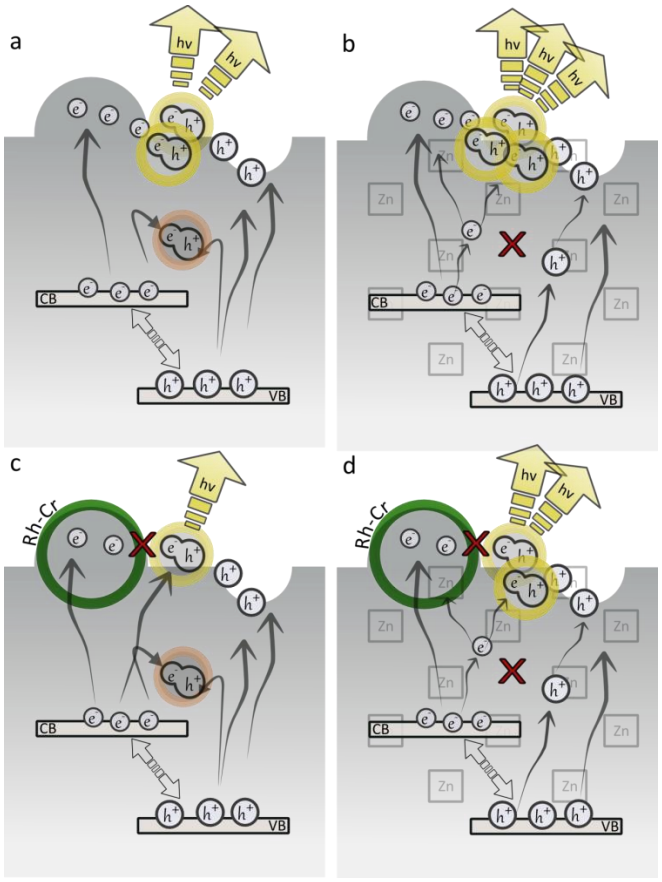

Fig. 11 Possible PL mechanisms induced by the promoters for a) bare Ga_2O_3, b) Ga_2O_3 Zn, c) Ga_2O_3 Rh-Cr, and d) Ga_2O_3 Zn/Rh-Cr. Yellow circles symbolize radiative recombination, red circles the non-radiative ones. The red crosses highlight the impeded recombination pathways after catalyst modification.

Rationalization of the promoter effects suggested by the PL experiments is illustrated in Fig. 11. In case of the bare catalyst, (Fig. 11a) a fraction of electron-hole couples generated by photoexcitation can independently migrate and get trapped in different localized states. Ultimately they will recombine either in a non-radiative (red circles) or radiative (yellow circles) way. Upon structural modification by zinc doping (Fig. 11b) the pathway of charge migration and confinement is altered, and different trapping states could be created. Zinc-promoted structures are suggested to block non-radiative recombination routes and reversely favour others. This results in populating alternative trap states finally leading to radiative recombination, particularly from the catalyst surface.

Rh-Cr particles are efficient traps of photoexcited electrons.[10] After Rh-Cr modification to the bare metal oxide (Fig. 11c), electrons from the conduction band efficiently migrate towards the Rh-Cr surface particles rather than staying at the long-living light emitting trap states. This could account for the observed PL decrease in presence of Rh-Cr particles. By co-modifying the catalyst with both Zn and Rh-Cr the combination of the two effects could be expected (Fig. 11d). Zn prevents charge recombination and Rh-Cr acts as an electron sink so that PL intensity and lifetime are only partially increased.

By integrating the catalytic results into this model, we can explain the specific roles of Zn and Rh-Cr, both contributing to boost H_2 and/or O_2 productivity by unique functions. Zinc acts as a buffer for photo-induced charge recombination, increasing lifetime of charged states and their surface concentration. On the other hand, Rh-Cr acts on a longer timescale in the mechanism and in competition with radiative recombination which seems directly related to the reducing power of O_2 to water. More specifically, Rh-Cr traps and protects photo-excited electrons from recombination, making them available exclusively for proton reduction. In short, zinc acts as a charge booster, while Rh-Cr would harvest electrons for H_2 evolution, preventing their use for O_2 reduction and thus enhancing O_2 production.

Conclusions

Zn, Rh-Cr, and Zn/Rh-Cr modified gallium, titanium, and tantalum oxides were successfully prepared and tested in a slurry reactor for overall water splitting reaction. A common productivity trend was consistently found in the order of bare oxide < Zn < Rh-Cr < Zn/Rh-Cr modified materials. The intrinsic activity of the metal oxides was also found to be extremely important, as the photocatalytic activity in terms of H_2/O_2 productivity can vary up to three orders of magnitude. Productivity values comparable level to the state-of-the-art (6.3 $mmol \cdot g^{-1} \cdot h^{-1}$ for our Ga_2O_3 Zn/Rh-Cr vs. ca. 20 $mmol \cdot g^{-1} \cdot h^{-1}$ of H_2 reported in batch)[7] were reached testing Ga_2O_3 materials. Tantalum based oxides also displayed excellent activity but with an order of magnitude below the promoted Ga_2O_3 materials. TiO_2 based materials, despite the fact that they are the most reported photocatalytic material, were more than 100 times less active than the gallium oxide based materials.

Under no circumstances CO_2, used as carrier gas, was found to be converted to gaseous reduced products, leaving the challenge open to further investigation.

Investigating in more detail the effect of doping and co-catalyst modifications, it appeared evident that the role of Rh-Cr is essential to consistently drive overall water splitting at high rate. Oxygen production was only observed in presence of the co-catalyst and also hydrogen production was equally boosted. This led to the hypothesis that Rh-Cr boosting mechanism relies on a dual action: enhancing hydrogen evolution (working with the classical electron trapping mechanism) and at the same time suppressing oxygen reduction, possibly by a simple coverage of Rh-Cr on the active sites, or effectively promoting the use of activated electrons towards hydrogen evolution and not towards oxygen reduction.

Zinc doping is certainly relevant for photocatalytic activity but in a totally different and less specific manner. Zinc doping alone does not trigger consistent oxygen evolution, and only marginally affects hydrogen one. However, its synergetic combination with Rh-Cr gives rise to the best catalytic activity in all catalyst modification series. This suggests that zinc might not be an active element of catalytic sites. Rather, it is actively involved in the process of formation of stable charge separation states after light excitation. Long living charges would then only fruitful acting in the catalysis in presence of an efficient surface charge trapping agent, namely Rh-Cr particles. Wavelength dependant catalytic tests showed that only highly energetic UV-C radiation below 275 nm can drive the photocatalytic process for both Ga and Ta oxides. This was expected for Ga_2O_3-based materials but not for Ta_2O_5-based materials whose bandgap should allow for a less energetic light activation. These results suggest that photocatalytic activity does not necessarily follow the widely accepted semiconductor mechanism.

UV-Vis diffuse reflectance spectroscopy revealed an inverse correlation between the range of spectral absorption of a material and its catalytic activity, i.e. materials with a smaller bandgap performed worse. Moreover, it appears that highly energetic UV-C excitation of a suitable material (Ga_2O_3) might be indispensable for boosting the quantum yields.

Photoluminescence (PL) spectroscopy and time resolved PL decay measurements provided detailed insights into the catalytic mechanism. PL intensity of Ta and Ga oxides family could be correlated to catalytic activity. Zn doping was found to have a relevant PL boosting effect with increased lifetime whereas Rh-Cr had a damping effect. These findings were associated with possible buffering of charge recombination by Zn and with electron trapping by Rh-Cr. The combination of these two effects would symbiotically account for the synergetic catalytic activity boost observed for Zn/Rh-Cr modified catalysts.

We demonstrated that PL techniques can be used as tool to rationalize photocatalytic activity. This is of particular relevance since the charge recombination dynamics is possibly the most important factor determining catalytic activity and quantum efficiency.[38] It is shown that proper evaluation of PL data and differentiating between doping and co-catalyst effects can be an effective tool to predict catalyst efficiency.

Acknowledgements

Financial support from the ICIQ Foundation, MINECO (CTQ2012-34153) and the Catalan government (2014 SGR 893) is greatly acknowledged. We also thank MINECO for support through Severo Ochoa Excellence Accreditation 2014-2018 (SEV-2013-0319).

Notes and References

1. A. Kudo and Y. Miseki, *Chem. Soc. Rev.*, 2009, **38**, 253-278.
2. M. Ni, M. K. H. Leung, D. Y. C. Leung and K. Sumathy, *Renew. Sustainable Energy Rev.*, 2007, **11**, 401-425.
3. R. Abe, *Photochem. Rev.*, 2010, **11**, 179-209.
4. X. Chen, S. Shen, L. Guo and S. S. Mao, *Chem. Rev.*, 2010, **110**, 6503-6570.
5. H. Kato, K. Asakura and A. Kudo, *J. Am. Chem. Soc.*, 2003, **125**, 3082-3089.
6. K. Maeda and K. Domen, *J. Phys. Chem. Lett.*, 2010, **1**, 2655-2661.
7. Y. Sakata, Y. Matsuda, T. Nakagawa, R. Yasunaga, H. Imamura and K. Teramura, *ChemSusChem*, 2011, **4**, 181-184.
8. Y. Sakata, Y. Matsuda, T. Yanagida, K. Hirata, H. Imamura and K. Teramura, *Catal. Lett.*, 2008, **125**, 22-26.
9. Y. Sakata, T. Nakagawa, Y. Nagamatsu, Y. Matsuda, R. Yasunaga, E. Nakao and H. Imamura, *J. Catal.*, 2014, **310**, 45-50.
10. K. Maeda, K. Teramura, H. Masuda, T. Takata, N. Saito, Y. Inoue and K. Domen, *J. Phys. Chem. B*, 2006, **110**, 13107-13112.
11. A. Bazzo and A. Urakawa, *ChemSusChem*, 2013, **6**, 2095-2102.
12. A. C. Taş, P. J. Majewski and F. Aldinger, *J. Am. Ceram. Soc.*, 2002, **85**, 1421-1429.
13. G. B. Kunshina, I. V. Bocharova, O. G. Gromov, E. P. Lokshin and V. T. Kalinnikov, *Inorg Mater*, 2012, **48**, 62-66.
14. R. D. Shannon and J. A. Pask, *J. Am. Ceram. Soc.*, 1965, **48**, 391-398.
15. R. Rodriguez-Talavera, S. Vargas, R. Arroyo-Murillo, R. Montiel-Campos and E. Haro-Poniatowski, *J. Mater. Res.*, 1997, **12**, 439-443.
16. T. Ohno, K. Sarukawa, K. Tokieda and M. Matsumura, *J. Catal.*, 2001, **203**, 82-86.
17. J. Porter, Y.-G. Li and C. Chan, *J. Mater. Sci.*, 1999, **34**, 1523-1531.
18. Y. Noda, B. Lee, K. Domen and J. N. Kondo, *Chem. Mater.*, 2008, **20**, 5361-5367.
19. K. Sayama and H. Arakawa, *J. Photochem. Photobiol., A*, 1994, **77**, 243-247.
20. Y. Takahara, J. N. Kondo, T. Takata, D. Lu and K. Domen, *Chem. Mater.*, 2001, **13**, 1194-1199.
21. J. N. Kondo, Y. Takahara, D. Lu and K. Domen, *Chem. Mater.*, 2001, **13**, 1200-1206.
22. J. B. Varley, J. R. Weber, A. Janotti and C. G. Van de Walle, *Appl. Phys. Lett.*, 2010, **97**, 142106.
23. J. Robertson and C. W. Chen, *Appl. Phys. Lett.*, 1999, **74**, 1168-1170.
24. Y. Matsumoto, *J. Solid State Chem.*, 1996, **126**, 227-234.
25. R. López and R. Gómez, *J Sol-Gel Sci Technol*, 2012, **61**, 1-7.
26. S. N. Habisreutinger, L. Schmidt-Mende and J. K. Stolarczyk, *Angew. Chem. Int. Ed.*, 2013, **52**, 7372-7408.
27. M. Anpo, H. Yamashita, K. Ikeue, Y. Fujii, S. G. Zhang, Y. Ichihashi, D. R. Park, Y. Suzuki, K. Koyano and T. Tatsumi, *Catal. Today*, 1998, **44**, 327-332.
28. B. Liu, L. Wen and X. Zhao, *Mater. Chem. Phys.*, 2007, **106**, 350-353.
29. K. Y. Jung, S. B. Park and M. Anpo, *J. Photochem. Photobiol., A*, 2005, **170**, 247-252.
30. J. Liqiang, Q. Yichun, W. Baiqi, L. Shudan, J. Baojiang, Y. Libin, F. Wei, F. Honggang and S. Jiazhong, *Sol. Energy Mater. Sol. Cells*, 2006, **90**, 1773-1787.
31. Y. Hou, L. Wu, X. Wang, Z. Ding, Z. Li and X. Fu, *J. Catal.*, 2007, **250**, 12-18.
32. T. Harwig and F. Kellendonk, *J. Solid State Chem.*, 1978, **24**, 255-263.
33. M. R. Hoffmann, S. T. Martin, W. Choi and D. W. Bahnemann, *Chem. Rev.*, 1995, **95**, 69-96.
34. V. M. Daskalaki, P. Panagiotopoulou and D. I. Kondarides, *Chem. Eng. J.*, 2011, **170**, 433-439.
35. N. M. Dimitrijevic, B. K. Vijayan, O. G. Poluektov, T. Rajh, K. A. Gray, H. He and P. Zapol, *J. Am. Chem. Soc.*, 2011, **133**, 3964-3971.
36. J. C. Colmenares and R. Luque, *Chem. Soc. Rev.*, 2014, **43**, 765-778.
37. K. Maeda, K. Teramura, D. Lu, N. Saito, Y. Inoue and K. Domen, *Angew. Chem.*, 2006, **118**, 7970-7973.
38. T. Hisatomi, K. Miyazaki, K. Takanabe, K. Maeda, J. Kubota, Y. Sakata and K. Domen, *Chem. Phys. Lett.*, 2010, **486**, 144-146.

Supporting Information

Understanding synergetic effects of Zn and Rh-Cr promotion to wide-bandgap Ga, Ta and Ti oxides in photocatalytic water splitting

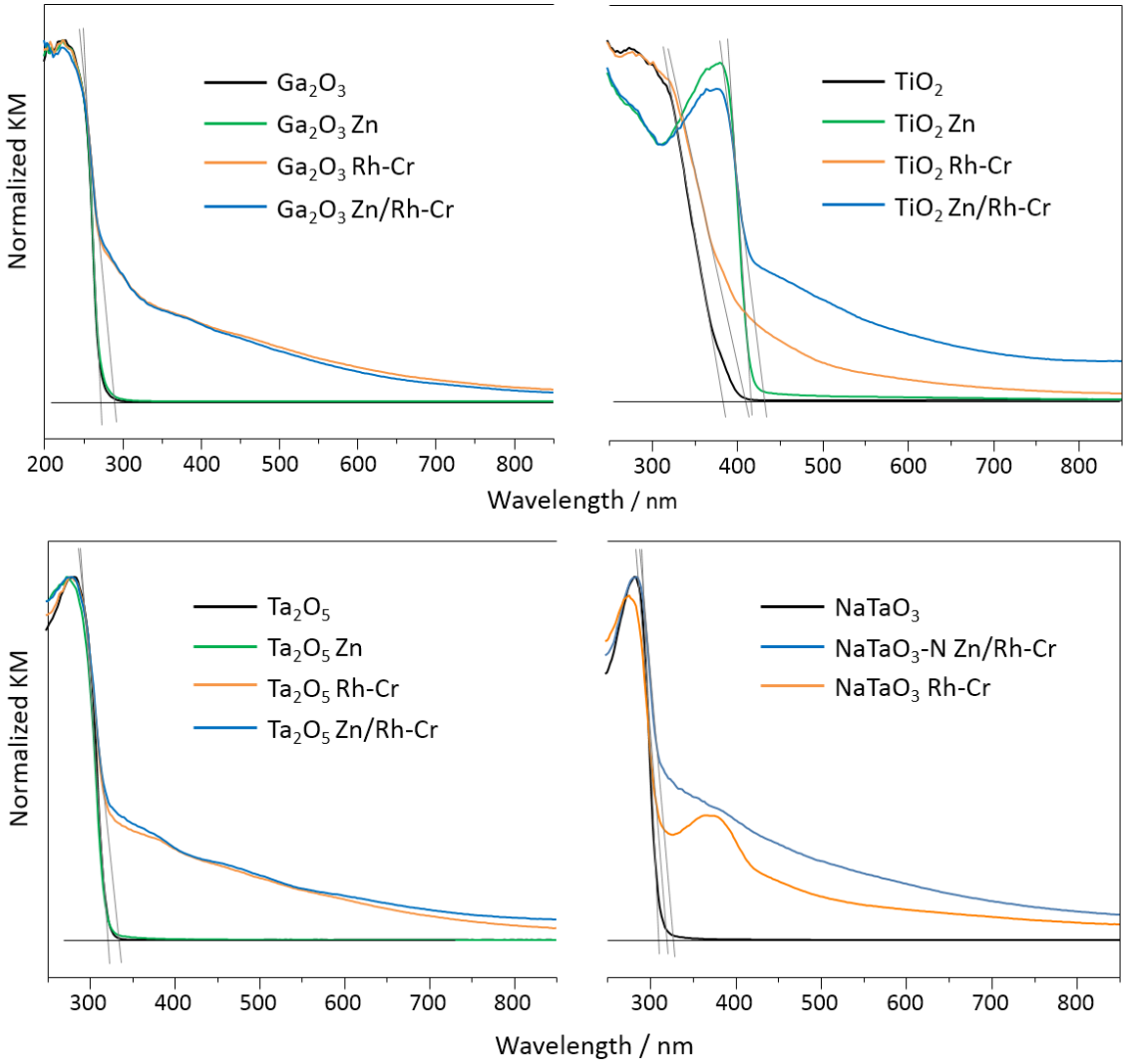

Figure S1. Diffuse reflectance KM plots of the used photocatalysts. Tauc plot intersecting lines are visualized in grey.

Table S1. KM plot derived λ_{onset} and corresponding Eg values (by the formula $Eg = 1240/\lambda_{onset}$).

Material	λ_{onset} /nm	E_g / eV	Material	λ_{onset} / nm	E_g / eV
TiO_2	382	3.25	Ta_2O_5	321	3.86
TiO_2 Zn	416	2.98	Ta_2O_5 Zn	321	3.86
TiO_2 Rh-Cr	409	3.03	Ta_2O_5 Rh-Cr	334	3.71
TiO_2 Zn/Rh-Cr	432	2.87	Ta_2O_5 Zn/Rh-Cr	334	3.71
Ga_2O_3	270	4.59	$NaTaO_3$-N	310	4.01
Ga_2O_3 Zn	270	4.59	$NaTaO_3$-N Zn/Rh-Cr	327	3.79
Ga_2O_3 Rh-Cr	290	4.28	$NaTaO_3$ Rh-Cr	319	3.89
Ga_2O_3 Zn/Rh-Cr	290	4.28			

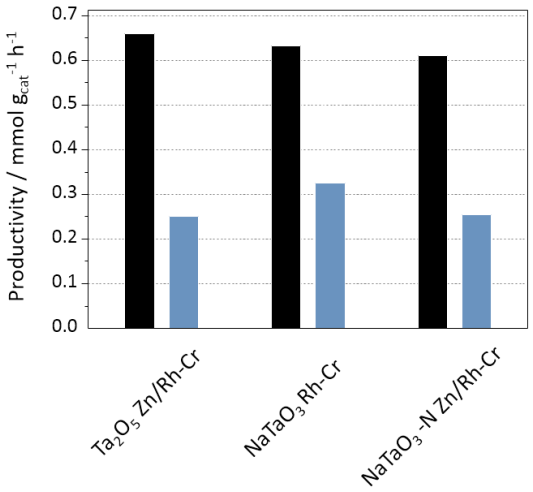

Catalyst	H_2	O_2
Ta_2O_5 Zn-Rh/Cr	0.66	0.25
$NaTaO_3$ Rh-Cr	0.63	0.32
$NaTaO_3$-N Zn/RhCr	0.61	0.27

Figure S2. Comparison of H_2 and O_2 steady-state productivity of Ta_2O_5 Zn/Rh-Cr, $NaTaO_3$ Rh-Cr and $NaTaO_3$-N Zn/Rh-Cr catalysts in slurry reactor (left), and correspondent H_2 and O_2 productivity (mmol·g^{-1}·h^{-1}) values (right).

During the course of our investigations, many tantalum based materials in the general form $MTaO_3$ (where M = Na or K) have been synthesized as promising candidates for overall water splitting. As further variety, different doping and co-catalyst impregnation have been attempted. La and N doping but also Cu, Fe, and Ti doping, using a hydrothermal synthesis approach. Ni, Pt, and Ru based co-catalyst impregnation on different tantalate substrate were also performed and these materials were tested for water splitting activity. $NaTaO_3$ materials were synthesized by urea combustion[1], and hydrothermal [2] techniques. Urea combustion $NaTaO_3$ samples were prepared from Ta_2O_5, Na_2CO_3, and $CO(NH_3)_2$ (molar ratio 1 : 1 : 4), mixed in a thick water slurry, dried at 353 K and crushed in a mortar. The urea blended precursors were then slowly heated (2 K/min) up to 573 K and subsequently brought to 873 K (5 K/min, 4 h).

Hydrothermal N-doped $NaTaO_3$ nanocubes were prepared in a Teflon lined autoclave. A Ta_2O_5, NaOH and NH_4OH (molar ratio 1 : 33 : 7.5) solution-suspension in water was prepared and heated at 453 K for 12 h under hydrothermal conditions. The solid product was then washed by centrifugation and dried at 353 K.

Contrarily to our expectation, no one of these materials was capable of overall water splitting activity or oxygen production in either slurry or gas phase. Hydrogen evolution productivity was in most case present, but at level in the range of bare Ta_2O_5, i.e. more than one order of magnitude inferior to data reported in literature for tantalate materials.

Remarkably different behaviour was observed for $NaTaO_3$-N Zn/Rh-Cr and $NaTaO_3$ Rh-Cr loaded catalysts. They exhibited excellent quasi-stoichiometric H_2 and O_2 evolution in slurry under UV irradiation.

The two Rh-Cr modified tantalum oxide display very similar catalytic activity. Especially, Zn doping does not seem to have any relevant (or even slightly negative) effect on the productivity. Even more importantly, the productivity is equivalent to what observed for Ta_2O_5 Zn/Rh-Cr, with a possible slight improvement in oxygen evolution (which gets closer to the desired stoichiometry). These findings showed that crystal structure only played a marginal role in determining the activity of Rh-Cr impregnated tantalum based materials, supporting a non-semiconductor-based mechanism. Other parameters, such as the presence of specific Ta-O surface active units, and their interaction with the Rh-Cr co-catalyst, could be better explaining the similar catalytic activity observed for the Ta_2O_5 and $MTaO_4$ materials.

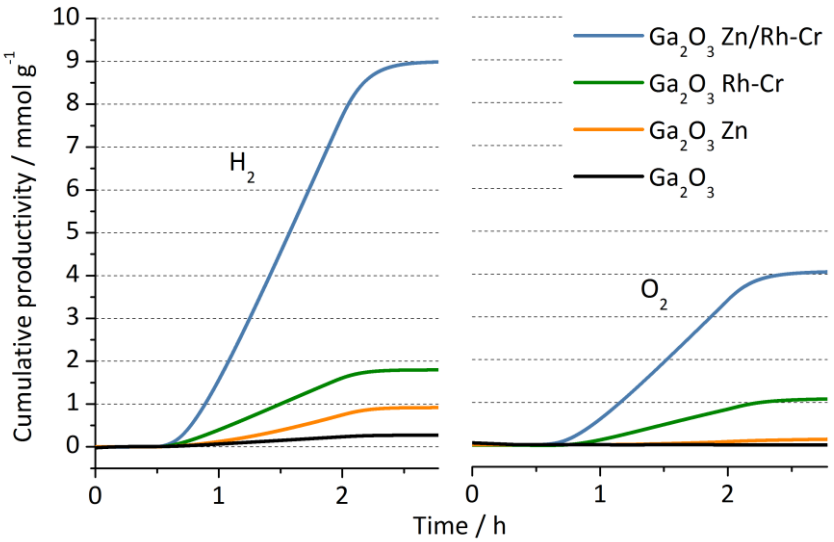

Figure S3. H_2 and O_2 cumulative productivity profiles with the unpromoted and promoted Ga_2O_3 catalysts in the continuous flow slurry reactor under 1.5 h UV (high pressure Hg lamp) irradiation (ON at 0.5 h, OFF at 2 h), calculated from the concentration profiles shown in **Fig. 3.**

1. J. Xu, Y. He, J. Zhang, J. Qian, D. Xu, X. He and D. Yang, *Micro & Nano Lett*, **2012**, *7*, 72-75.
2. H. Fu, S. Zhang, L. Zhang and Y. Zhu, *Mater. Res. Bull.*, **2008**, *43*, 864-872.